

## **Effect of Fe<sup>3+</sup>-MMT on thermal degradation and mechanical behavior of PVP/Amylose nanocomposite films**

Naser Sadeghpour Orang<sup>1</sup> and Reza Abdollahi<sup>\*2</sup>

<sup>1</sup> Faculty of Technical Engineering, Department of Chemical Engineering, IAU, Ahar, Iran

<sup>2</sup> Chemistry Department, South Tehran Branch, Islamic Azad University, Tehran, Iran

Received January 2019; Accepted August 2019

### **ABSTRACT**

Novel nanocomposite films based on amylose (AM) and Fe<sup>3+</sup>-montmorillonite (Fe<sup>3+</sup>-MMT) in the matrix of poly (vinyl pyrrolidone) (PVP) were fabricated by using a solution casting method. The X-Ray diffractational analysis indicated that an ion-exchange process occurred between Fe<sup>3+</sup>-MMT and PVP. Thermogravimetric analysis (TGA), differential thermogravimetric analysis (DTG), Scanning Electron microscopy (SEM) and differential scanning calorimetry (DSC) results hinted to PVP/AM films forming a stabler network through the dispersion of Fe<sup>3+</sup> cations. An increase in the loading of Fe<sup>3+</sup>-MMT improved the hydrophilic properties of PVP/AM films, which lead to the high degree of resistance against on the water absorption. Mechanical properties of PVP/AM films influenced by the uniform dispersion of Fe<sup>3+</sup>-MMT in polymer network established with strong covalent interactions between PVP/AM and Fe<sup>3+</sup>-MMT. This interaction not only improved the mechanical properties of the films, but also enhanced the thermal stability of them through the facilitating of the MMT dispersion within the polymer matrix.

**Keywords:** Amylose; PVP, PVP/AM film; Fe<sup>3+</sup>-MMT Nanocomposite; thermal stability; glass transition temperature (T<sub>g</sub>)

## **1. INTRODUCTION**

Recently, various methods have been considered to prepare temperature-sensitive hydrogels which improved mechanical properties [1-3], while the electrical behavior of the developed hydrogels has been evaluated by investigation on the charge transferring that might be occurring between the matrix components [4]. These types of hydrogels have been studied to produce membranes with high compatibility in the biological systems [5, 6]. PVP is a potential material for using in these systems because of its favorable environmental stability, easy process situation, excellent transparency

and having a good charge storage capacity [7]. Also PVP is an amorphous polymer, and it is known to form various complexes with many inorganic salts due to the presence of the rigid pyrrolidone groups [8]. However, combination of PVP with amylose may led to modified mechanical properties via synergistic effects between these two polymers [9]. The ability of amylose for the formation of amylose-small molecule's complex is approved to be a great interest in a wide variety of fields, including drug delivery and biomedical industries [10]. Therefore, the combination of PVP and amylose provides

---

\*Corresponding author: r.abdollahi@Tabrizu.ac.ir

a new type of composites with its competitive behavior of components enhanced by participation of metal cations. Polymer/clay nanocomposites (PCNs) represent a new class of materials which their properties depend on the special distribution, rearrangement of intercalating polymer chains, and type of interactions between polymer and clay [11, 12]. Fe<sup>3+</sup>-montmorillonite (Fe<sup>3+</sup>-MMT) can be synthesized by ion-exchange reaction with sodium montmorillonite. The interlayer structure of MMT embedded metal cations in its matrix improves the hydrophobicity properties leading to a high degree of swelling in water [13]. These phenomena provided an efficient method for preparing intercalated nanocomposites in the case of using aqueous media during the process. Amylose is a neutral carbohydrate polymer and certainly the hydroxyl group's oxygen can donate the negative charge to Fe<sup>3+</sup> through an electrostatic action. Also the PVP have a strong negative charge on the backbone of the polymer chain due to the amide and hydroxyl groups. Thus, the composite of PVP/AM could interact with Fe<sup>3+</sup>-MMT, which has a positive charge in the interlayer lattice. The Fe<sup>3+</sup>-MMT can be considered as a source of positive charge that could be approached to the metal cations through the polymer chain, when they close to the polymer network [14]. Many reports mention that Fe-clay was used as an effective Fenton catalyst in the case of photocatalytic processes [15, 16]. This particular study focuses on the difference of mechanical properties of PVP/AM, PVP/AM/MMT and PVP/AM/Fe<sup>3+</sup>-MMT films, an investigation on the relevant thermal behavior using thermogravimetry analysis, and differential scanning calorimetry. The ion-exchange process between Fe<sup>3+</sup>-MMT and PVP/AM was confirmed by X-ray diffraction (XRD). Results indicated that the presence of Fe<sup>3+</sup>-MMT in matrix of

PVP/AM improved the mechanical properties and modified the thermal stability of fabricated polymer composite.

## 2. MATERIALS AND METHODS

### 2.1. Materials

Amylose (C<sub>6</sub>H<sub>10</sub>O<sub>5</sub>)<sub>n</sub> was purified from potato starch, with purity of 99% was purchased from Gamay industrial technology Co. Ltd, Shanghai-China (number average molecular weight 48600 Da). Poly (vinyl pyrrolidone) (PVP) (average molecular weight 58000 Da), Ferric chloride hexahydrate (FeCl<sub>3</sub>·6H<sub>2</sub>O, >99%), and ammonium hydroxide (NH<sub>4</sub>OH, M<sub>w</sub>=35.05) were purchased from Fluka (Switzerland). Sodium montmorillonite (Cloisite Na<sup>+</sup>) with a cation exchange capacity (CEC) of 92.6 mequiv./100 g clay was supplied by Nanocor Inc. (Arlington Heights, IL). Distilled water was used throughout of the work.

### 2.2. Preparation of PVP/AM film

The procedure of preparing PVP/AM films was as follows: 2g amylose powder was dispersed into 50mL of distilled water. 30mg glycerol was added to the amylose suspension with stirring. A solution of PVP in aqueous ammonium hydroxide was prepared by stirring 8g of PVP in 100 g of concentrated ammonium hydroxide-water in a flask equipped with a stirrer and reflux condenser. The obtained mixture was heated to 100°C, stirred for 2hrs and it was allowed to be cooled down. This solution was also added to the amylose suspension and prepared mixture was undergoing ultrasonic treatment for 15min, and then was stirred at 100°C for 60min until the mixture became a homogeneous and semi-transparent solution. After degassing, the solution was poured onto a plate and was dried by airing at room temperature for four days to form a film. Finally, the PVP/AM films were peeled off the plate

and were stored for further analysis.

### 2.3. Preparation and dispersion of Fe<sup>3+</sup>-MMT

1g of Na<sup>+</sup>-MMT and 0.057g of FeCl<sub>3</sub> were dissolved in 60ml of deionized water by stirring for 12hr(s) at 70 °C. The solution was then filtered and was dried in a vacuum oven at 40 °C for 1 day. 1g of obtained Fe<sup>3+</sup>-MMT was dispersed in 60 ml of deionized water for swelling by stirring for 12hr(s) at 70 °C.

### 2.4. Preparation of PVP/AM/Fe<sup>3+</sup>-MMT nanocomposites

PVP/AM/Fe<sup>3+</sup>-MMT films with the different amounts of Fe<sup>3+</sup>-MMT loadings (1, 3 and 5 wt %) were processed. At first step the 2g amylose was dispersed into 200 mL distilled water and g PVP were added into the solution and also the desired amount of Fe<sup>3+</sup>-MMT was added to the solution, subsequently. In this case, the desired mass ratios of PVP-AM/Fe<sup>3+</sup>-MMT: 99/1, 97/3 and 95/5 were achieved. Then the prepared suspensions were exposed at ultrasonic radiation in 30W power of sonication at the aqueous media for 30h and stirred simultaneously in a fixed temperature by means of a thermostat at 30°C. The thin films that resulted after heating at 50°C for 5h in a vacuum oven could be lifted easily from the PVC plates. The films were dried further at 40 °C for 1 day.

### 2.5. Moisture content determination

The moisture contents of both the PVP/AM films alone and in the presence of Fe<sup>3+</sup>-MMT nanocomposites were determined by a gravimetric method. The measurements were performed in the environment of saturated KBr salt solution to attain the relative humidity (RH) almost at 81%. The initial weight of dry films was determined after getting dried to a constant weight in a vacuum oven at 60°C for

24hr(s). The weighed samples were then placed in incubators at 25°C, and they were weighed at intervals until their weights were become constant. The tests were conducted in triplicates, and average values were reported. The value of moisture absorbability (Ma) was calculated as Eq.1:

$$Ma\% = \left[ \frac{W - W_0}{W_0} \right] \times 100 \quad (1)$$

### 2.6. Tensile test of films

The tensile tests of the obtained films were measured at room temperature by using a special tensile testing system (Instron, 6025). A specific dumbbell-shaped specimen geometry was used to localizing the deformation in the region where all the mechanical variables were determined.

### 2.7. Characterization

#### 2.7.1. Differential scanning calorimetry (DSC)

The T<sub>0</sub>, T<sub>p</sub>, T<sub>c</sub> and ΔH of the films were determined by DSC thermograms. The samples were analyzed by using of Pyris 1 DSC (Perkin Elmer, USA). The system was calibrated for temperature and heat flux with Indium (transition point: 156.6°C, heat of fusion=3.28 kJ mol<sup>-1</sup>). The samples (8–15 mg) were weighed in Aluminium pans and hermetically were sealed. Then, an empty pan was used as the reference. Scans were carried out over the temperature range of 0-280°C at a heating rate of 10°C/min<sup>-1</sup> under Nitrogen atmosphere. During each run, the flow rate of nitrogen was 24cm<sup>3</sup>/min.

#### 2.7.2. Dynamic mechanical analysis (DMA)

A DMA 242 C (Netzsch, Germany) was used to measuring the glass transition temperature of samples (approximately 10.00×10.00 mm) PVP/AM/Fe<sup>3+</sup>-MMT nanocomposite films. The samples were

fixed by the clamp without relaxation and deformation. Also the surface of the films was coated with silicon oil to reduce moisture loss during the measurement. The system was run in the rectangular tension mode at 1 Hz, with a temperature range of between 0 and 90 °C at a heating rate of 3 °C/min.

### 2.7.3. X-ray diffraction

X-ray diffraction analysis was performed with a Siemens XRD-5000 diffractometer operated at 40 kV, 50 mA at 25°C with a graphite-filtered Cu K $\alpha$  = 1.54Å target radiation. The relative intensity was recorded in the scattering range (2 $\theta$ ) of 0–30°.

### 2.7.4. Thermogravimetric analysis

The thermal gravimetric analysis (TGA) curves of the nanocomposite films were obtained by a Perkin Elmer Pyris TGA-DTG analyzer. The applied temperature range was 25-600°C under nitrogen atmosphere flow of 20cm<sup>3</sup>/min with a heating rate of 10°C/min for 3-5 mg samples. Before measuring, the films were first dried in a vacuum to get a constant weight at 60°C. The weight of each sample was approximately 20mg. For each sample, the following parameters were determined: the maximum temperature of degradation (T<sub>max</sub>), the temperature that 10% weight loss occurred (T<sub>90</sub>), the onset temperature (T<sub>onset</sub>), that denotes the temperature of starting the weight loss and the residual mass at 600 °C (RM600). The MC100, T<sub>onset</sub> and RM600. The values were estimated from the dependence of the mass loss on temperature (TG curves), and the T<sub>max</sub> values were taken as the maximum of the first-order derivative curves of mass loss to temperature (DTG curves).

### 2.7.5. Scanning electron microscopy (SEM)

The morphology of the surface of the films was investigated by using a scanning electron microscope. The sample was coated with pure Au by using a sputter coater (SCD500 sputter coater, Bal-Tec, Switzerland). The laying down of Ag was carried out by using the evaporation of the metal under a high vacuum to give a thickness of about 100Å. The samples were observed and were photographed in an environmental SEM (PhlipsXL-30) with an accelerating voltage of 30kV and working distance of 10mm.

## 3. RESULTS AND DISCUSSION

### 3.1. Study of microstructure of PVP/AM/Fe<sup>3+</sup>-MMT nanocomposite films

The structure and mechanism of ion-exchange phenomena in the polymer matrix are illustrated in Fig. 1. The positive nature of Fe<sup>3+</sup> cations due to the three positive charges makes it possible to intercalate through the MMT network. When Fe<sup>3+</sup> cations in the interlayer of MMT were replaced with NH<sub>4</sub><sup>+</sup>, the Fe<sup>3+</sup> ions are free from MMT. The released Fe<sup>3+</sup> cations in the vicinity of PVP/AM negative matrix might have a great potential to form a network with covalent interactions.

Fig. 2 shows XRD patterns of the Fe<sup>3+</sup>-MMT, pure amylose, PVP separately as the PVP/AM blend, and MMT incorporated PVP/AM films. As it has been shown in fig. 2(a) and (b), the XRD pattern obtained from initial Amylose and PVP, showed an essentially diffused pattern for amorphous materials. Amylose presents three main diffraction peaks at 11°, 15° and 24° [17, 18]. In addition, some conditions such as blending process and increasing in temperature could change the crystalline shape of amylose as were described by X. Zhou et al. [19]. As it has been shown in Fig. 2(b), the typical pattern of PVP is a B-type pattern whereas

the diffraction pattern of PVP/AM in Fig. 4(c) was a V- type pattern with peaks at 17° and 19° as were described by Taghizadeh et al. [20]. Furthermore, Ryno et al. reported a  $V_h$  polymorph crystalline shape for Amylose molecules that was prepared by microwave irradiation [21]. They found that amylose molecules after the formation of complex change the B-type pattern to the V-type crystalline shape [22, 23]. The main peak in the diffraction pattern of the MMT was attributed to the formation of the interlayer spaces by regular stacking of the silicate layers along the [0 0 1] direction [24]. The XRD pattern of  $Fe^{3+}$ -MMT illustrated in Fig. 2(e) and the principle reflection peak is appeared at 11°. In the case of PVP/AM/  $Fe^{3+}$ -MMT nanocomposite the interlayer distance was

related to separation of the PVP/AM chains due to the intercalation of  $Fe^{3+}$ -MMT into the interlayer of composite network (Fig. 2(d)) which this phenomenon was observed by the peak shift to approximately 17°. The reason of this peak shifting is related to the presence of  $Fe^{3+}$  cations in the interlayer of MMT nanosheet structure that were replaced with  $NH_4^+$  ions. The uniform dispersion of  $NH_4^+$ -MMT in the PVP/AM matrix assisted to good intercalation of  $Fe^{3+}$  through the cation replacement process. The decrease of the peak intensity in the case of PVP/AM/  $Fe^{3+}$ -MMT is considerable rather than the initial pattern resulted by exfoliation of MMT to the composite films.

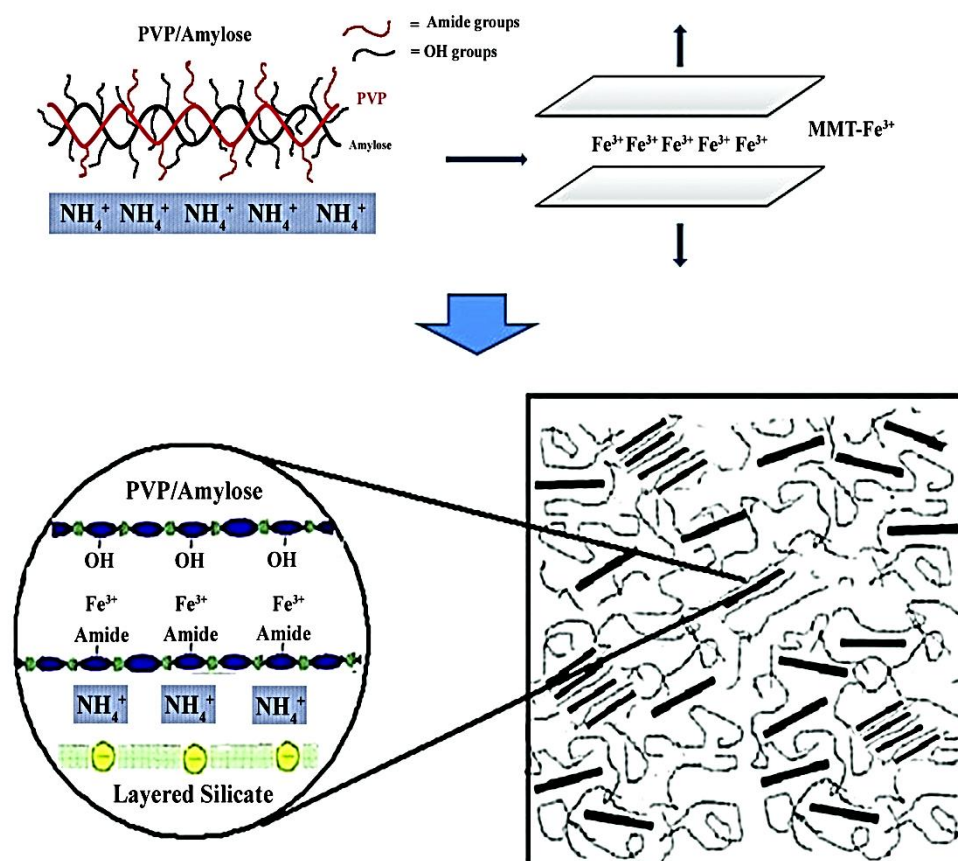


**Fig. 1.** Mechanism of formation of PVP/AM/  $Fe^{3+}$ -MMT nanocomposite.

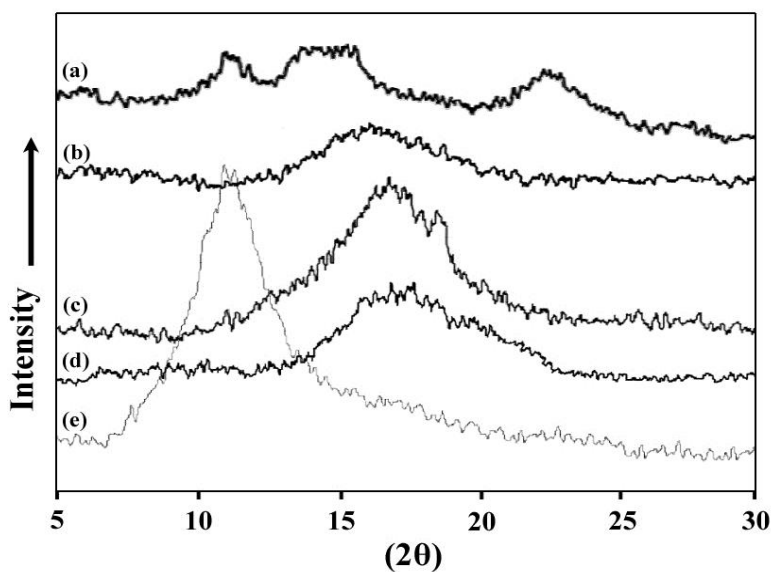


**Fig. 2.** XRD diffractograms for pure amylose (a), pure PVP (b), PVP/AM blend composite (c), as well as PVP/AM/  $\text{Fe}^{3+}$ -MMT (d) and  $\text{Fe}^{3+}$ -MMT (e) nanocomposites.

### 3.2. Weight loss and water uptake of the PVP/AM/ $\text{Fe}^{3+}$ -MMT nanocomposite films

The water absorption capacity of amylose is very considerable because of the hydroxyl groups which are located on its molecular structure. However, Zhang et al. reported that the copolymer based on starch with lower content of amylose represents higher water absorbency behavior [25]. The water absorption capacities of the PVP/AM/ $\text{Fe}^{3+}$ -MMT nanocomposite films were found to have significant differences, and were consistent with the results of Taghizadeh et al. [26]. The increase of  $\text{Fe}^{3+}$ -MMT nanocomposite loading leads to the decrease of water uptake. Fig. 3(a) and Table 1 clearly showed that moisture absorbability is much more pronounced when the PVP/AM composite films are in the pure state and addition of  $\text{Fe}^{3+}$ -MMT decreased the water absorbability of the films. The hydroxyl groups of  $\text{Fe}^{3+}$ -MMT can form strong hydrogen bonds with the hydroxyl groups on amylose, and with the amide groups on PVP. [27]. Furthermore, the

MMT sheets produce a twisted pathway and diminish the length of the free passage for water absorption. Almasi et al. have studied the water absorption of starch/CMC/nanoclay composite films and showed that nano-fillers improved the water resistance of the composite films [28]. These results suggest that the addition of  $\text{Fe}^{3+}$ -MMT improves the water resistance of the PVP/AM films. The Fig. 2(b) indicated the weight loss of PVP/AM films in the presence of  $\alpha$ -amylase, and confirmed the water barrier nature of  $\text{Fe}^{3+}$ -MMT nanocomposite which led to less access of water molecules to the bulk of PVP/AM network. Therefore, the enzymatic hydrolysis of composite films, which must be occurring in the aqueous media, does not be terminated. Fig. 4 shows the SEM pictures of the surfaces of intact PVP/AM (80:20) (A), PVP/AM/ $\text{Fe}^{3+}$ -MMT(5wt.%) (B), PVP/AM/ $\text{Fe}^{3+}$ -MMT (3wt. %) (C), and PVP/AM/ $\text{Fe}^{3+}$ -MMT (1wt. %) (D) After enzymatic degradation for 60hr(s). In the case of lower content of  $\text{Fe}^{3+}$ -MMT, the porosity of the film is considerable.

Nevertheless, in the case of 5wt. % of added nanocomposite, the surface of the film is relatively smoother. In the case of high loading of Fe<sup>3+</sup>-MMT, the enzyme molecules of  $\alpha$ -amylase hardly absorb on the PVP/AM films surface. The lamella nature of MMT nanosheets made the pathway of water molecule's complicated

diffusion and caused low porous surface resulted from hydrolysis of polymer bulk. The results may be applicable in the environmental concerning investigations to introduce new series of biodegradable materials with ability of degradation rate controlling option [29]

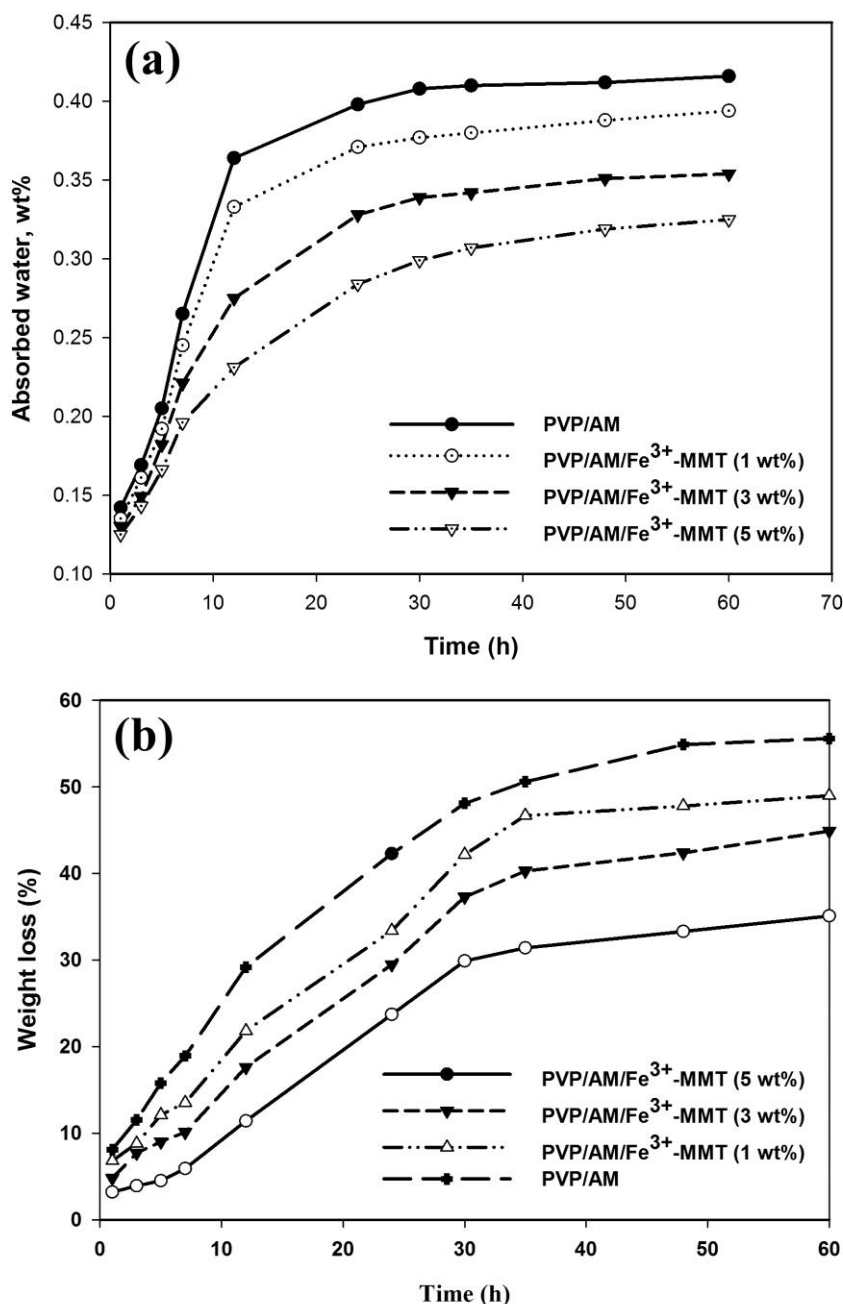


**Fig. 3.** Water uptake (a) and weight loss of PVP/AM/Fe<sup>3+</sup>-MMT films with different amounts of Fe<sup>3+</sup>-MMT nanocomposite and in the presence of 1mg of  $\alpha$ -amylase enzyme.

**Table 1.** A summary of the moisture absorbability of PVP/AM/Fe<sup>3+</sup>-MMT films in the presence of different amount of Fe<sup>3+</sup>-MMT nanocomposite

Time (h)	Fe <sup>3+</sup> -MMT loadings at PVP/AM blend (wt %)			
	0%	1%	3%	5%
	Moisture absorbability (Ma %)			
1	14.2	13.5	13.0	12.5
3	16.9	16.1	14.9	14.3
5	20.5	19.2	18.2	16.6
7	26.5	24.5	22.1	19.6
12	36.4	33.3	27.5	23.1
24	39.8	37.1	32.8	28.4
30	40.8	37.7	33.9	29.9
35	41.0	38.0	34.2	30.7
48	41.2	38.8	35.1	31.9
60	41.6	39.4	35.4	32.5

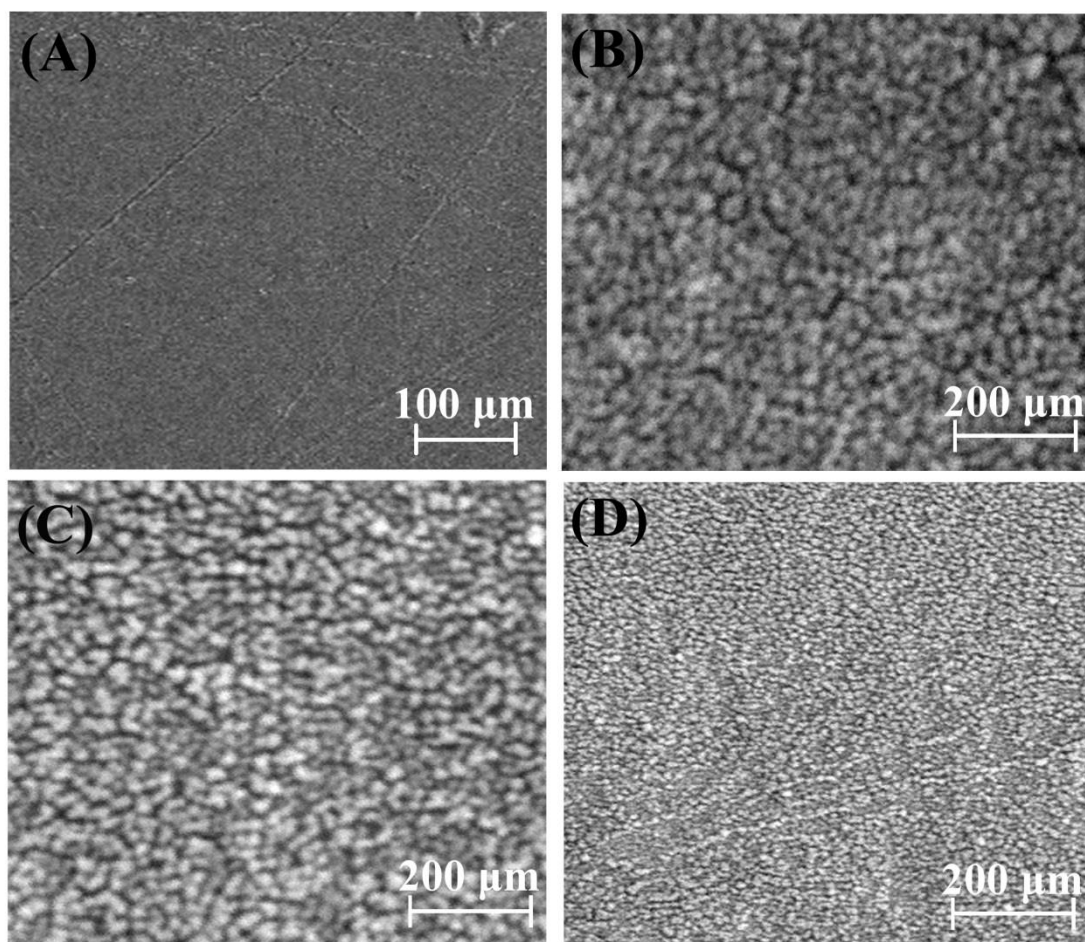


**Fig. 4.** Scanning electron micrographs of initial PVP/AM films (A) and PVP/AM/Fe<sup>3+</sup>-MMT nanocomposite films containing 5wt.% (B), 3 wt.% (C) and 1 wt.% of Fe<sup>3+</sup>-MMT.

### 3.3. Mechanical properties of PVP/AM/Fe<sup>3+</sup>-MMT nanocomposite films

It is known that interaction among polymers should influence the mechanical properties of the composite polymeric materials. In generally, mechanical properties of materials are strongly influenced by the microstructure, and they could provide important information about the internal structure of materials [30]. The tensile properties for neat PVP/AM composite films in different ratios of PVP/AM (90:10, 80:20, 70:30, and 60:40) and also for PVP/AM/Fe<sup>3+</sup>-MMT nanocomposite films loaded by 1, 3 and 5 wt% of Fe<sup>3+</sup>-MMT nanocomposite which were investigated. The results of obtained mechanical parameters included (a) the Young's modulus, (b) tensile strength (defined as the stress at break), and (c) elongation at break are illustrated in Fig. 5. The Young's modulus of the PVP/AM represented a modified amount when the amylose content rised from 10% to 20% that increased from 58.65 MPa to 177.23 MPa (Fig. 5a). Moreover, the Young's modulus of the PVP/AM/Fe<sup>3+</sup>-MMT nanocomposite films improved with increasing Fe<sup>3+</sup>-MMT loading. The significant enhancement of Young's modulus could be related to the hydrogen

bonds formed between the PVP/AM and the MMT nanosheets which act as bridges to link the MMT nanosheets and the PVP/AM matrix. The exerted force on the PVP/AM/Fe<sup>3+</sup>-MMT film was transferred to the MMT nanosheets through the hydrogen bonds and dissipated (Fig. 5b). The tensile strength of PVP/AM/Fe<sup>3+</sup>-MMT showed significant improvement when the amount of Fe<sup>3+</sup>-MMT nanocomposite increased to 5 wt% (Fig. 5c and Table 2). Such behavior is attributed to water molecules that act as a plasticizer and in the case of high Fe<sup>3+</sup>-MMT loading, the amount of the intermolecular absorbed water reduced. At high moisture absorption the more water molecules absorbed by PVP/AM/Fe<sup>3+</sup>-MMT nanocomposite films the more the tensile strength decreased [31] (Fig. 5d).

A Significant decrease in the elongation at the break compared to PVP/AM was observed. This was related to the aggregate formation of Fe<sup>3+</sup>-MMT within the polymer matrix. On the other hand, the hybrid nanocomposite filled with 3wt% Fe<sup>3+</sup>-MMT shown an elongation at break of 80%, which increased significantly compared to PVP/AM. These dramatic improvements were attributed to the fine dispersion of Fe<sup>3+</sup>-MMT in the polymer matrix [32].

**Table 2.** Comparison of mechanical properties of the PVP/AM/Fe<sup>3+</sup>-MMT films with different amounts of Fe<sup>3+</sup>-MMT nanocomposite

Sample	PVP/AM (% ratio)	Young's modulus (MPa)	Tensile strength (MPa)	Elongation at break (%)
PVP/AM	100:0	44.3	-	-
	90:10	58.5	-	-
	80:20	177.2	6.4	59.2
	70:30	190.3	-	-
	60:40	202.4	-	-
	50:50	219.0	-	-
PVP/AM/Fe <sup>3+</sup> -MMT (1 wt %)	80:20	181.4	7.9	72.1
PVP/AM/ Fe <sup>3+</sup> -MMT (3 wt %)	80:20	205.3	9.5	83.2
PVP/AM/ Fe <sup>3+</sup> -MMT (5 wt %)	80:20	286.6	13.0	23.1

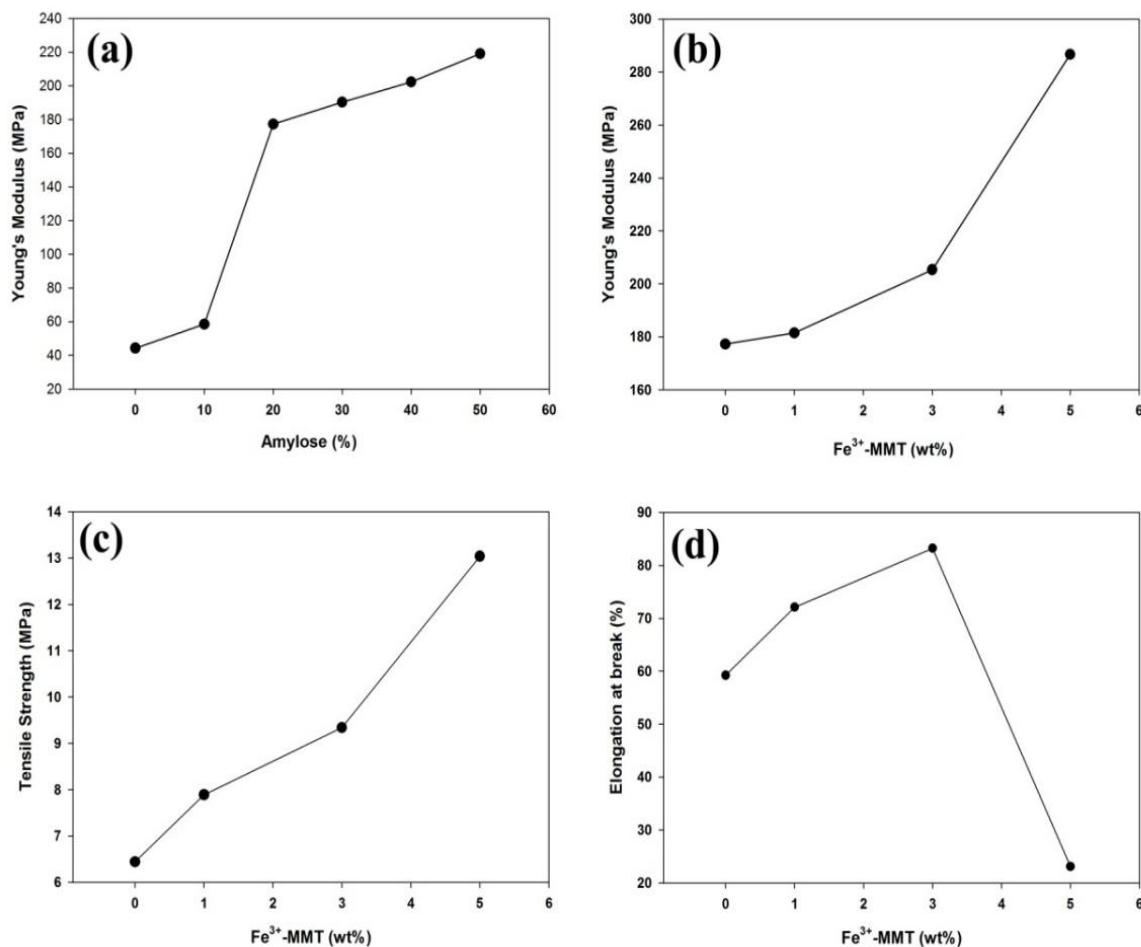


**Fig. 5.** Mechanical properties of PVP/AM/Fe<sup>3+</sup>-MMT nanocomposite films. The Young's modulus of films with different ratios of PVP: amylose (a), and for PVP/AM/ Fe<sup>3+</sup>-MMT nanocomposite films (b); tensile strength (c) and elongation at break (d) with different amounts of Fe<sup>3+</sup>-MMT nanocomposite.

### 3.4. Thermal properties of PVP/AM/ Fe<sup>3+</sup>-MMT nanocomposites

The first heating thermograms obtained during melting of pure amylose and PVP and related composite and nanocomposites with different content of Fe<sup>3+</sup>-MMT is presented in Fig. 6. Also, the endothermic data containing onset temperature ( $T_0$ ), peak temperature ( $T_p$ ), and enthalpy ( $\Delta H$ ) are shown in Table 3. At the constant ratio of PVP/AM composite film (80:20) the amount of  $T_0$ ,  $T_p$  and  $T_c$  has been shown to be influenced by Fe<sup>3+</sup>-MMT content.  $T_0$  and  $T_p$  temperatures rise with increase in the content of Fe<sup>3+</sup>-MMT. This may be

related to the structure of Fe<sup>3+</sup>-MMT nanocomposite structure that gave a lamella nature to the PVP/AM/Fe<sup>3+</sup>-MMT nanocomposite film that modified the thermal behavior of the films by an increasing the crystallinity of the nanocomposite matrix [33, 34]. The changes in  $T_0$  of PVP/AM/Fe<sup>3+</sup>-MMT with different Fe<sup>3+</sup>-MMT loadings were less obvious, while the  $T_0$  of PVP/AM/Fe<sup>3+</sup>-MMT (1wt %) is obviously higher than PVP/AM composite film. In the case of peak temperature, the value of  $T_p$  enhanced with increasing the loading of Fe<sup>3+</sup>-MMT nanocomposite and was

similar to the change in  $T_0$  of PVP/AM/Fe<sup>3+</sup>-MMT nanocomposite [35]. In addition, the pure amylose film had higher enthalpy, which corresponded to the presence of some of the granular structure

remained within the thermal analysis that acted as a self-reinforcing filler and enhanced the thermal properties of initial amylose films. This was consistent with the results of M. Li et al. [36].

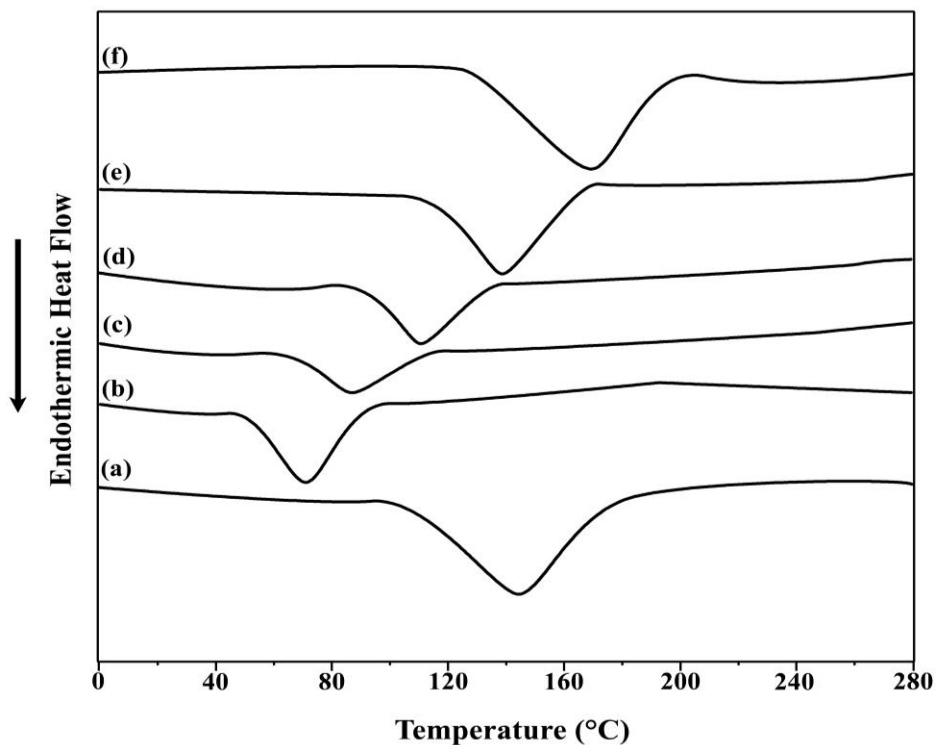


**Fig. 6.** DSC thermograms for (a) pure amylose, (b) pure PVP, (c) PVP/AM blend, and for PVP/AM/Fe<sup>3+</sup>-MMT nanocomposites containing (d) 1wt%, (e) 3wt% and (f) 5wt% of Fe<sup>3+</sup>-MMT nanocomposite.

**Table 3.** Gelatinization characteristics of different samples obtained by DSC analysis

Sample	$T_0$ (°C)	$T_p$ (°C)	$T_c$ (°C)	$T_c-T_0$ (°C)	$\Delta H$ (J/g)
Pure Amylose	100.34	143.78	192.43	92.09	7.22
Pure PVP	46.25	71.31	96.53	50.28	3.20
PVP/AM (80:20)	53.40	87.81	117.27	63.87	3.46
PVP/AM/ Fe <sup>3+</sup> -MMT (1wt %)	86.10	109.20	146.20	60.10	4.72
PVP/AM/ Fe <sup>3+</sup> -MMT (3wt %)	105.67	137.65	170.02	64.35	6.56
PVP/AM/ Fe <sup>3+</sup> -MMT (5wt %)	110.84	154.25	198.38	87.54	6.62

One of the other important parameters that should be evaluated in polymeric materials is glass transition temperature ( $T_g$ ). Liu et al. reported that detecting of  $T_g$  for starch-based materials by DSC is so complicated [37]. The  $T_g$  of the pure

amylose, pure PVP, PVP/AM composite films and PVP/AM/Fe<sup>3+</sup>-MMT in different conditions was investigated by DMA and the results are illustrated in Fig. 7 which indicated the  $T_g$  of samples in the range of 30-50°C. P. Liu et al. also used DMA

method to investigate the  $T_g$  of starch films with different amylose/amylopectin ratios [38]. They found that  $T_g$  was increased from about 52 to 60°C with increasing amylose content from 0% to 80% for the samples containing about 13% moisture. These findings confirmed that the  $T_g$  of starch is corresponded to the relative humidity (RH) and also the ratio of

amylose/amylopectin of starch films [39]. As seen, the  $T_g$  of PVP/AM (80:20) blend showed a single glass transition temperature between the  $T_g$  of pure amylose and PVP. The state of  $T_g(\text{PVP}) < T_g(\text{PVP/AM}) < T_g(\text{amylose})$  indicated the miscibility of two polymer in the composite matrix [40]

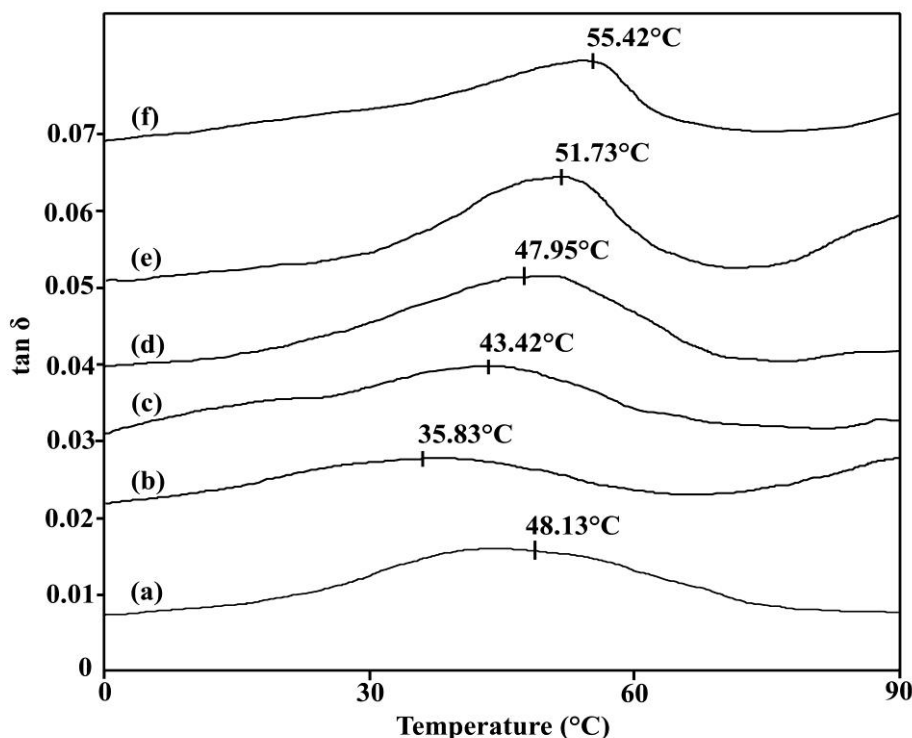


**Fig. 7.** DMA results for (a) pure amylose, (b) pure PVP, (c) PVP/AM blend, and for PVP/AM/  $\text{Fe}^{3+}$ -MMT nanocomposites containing (d) 1wt%, (e) 3wt% and (f) 5wt% of  $\text{Fe}^{3+}$ -MMT.

Also; the  $T_g$  of binary polymeric systems can be estimated by using Fox's equation [Eq. 2] [41], or Wood's equation [Eq. 3] [42].

$$\frac{1}{T_g} = \frac{X_1}{T_{g1}} + \frac{X_2}{T_{g2}} \quad (2)$$

$$T_g = W_1 T_{g1} + W_2 T_{g2} \quad (3)$$

Where  $X_1$ ,  $X_2$ ,  $T_{g1}$  and  $T_{g2}$  are the weight fractions and glass transition

temperature of the corresponding to polymer 1 and polymer 2, respectively. The experimental value of  $T_g$  for PVP/AM (80:20) blend compared with theoretical values are summarized in Table 4. The experimental  $T_g$  value of PVP/AM blend was slightly higher than that of theoretically calculated values and implying an intermolecular interaction between the polymers [43].

**Table 4.** Experimental and theoretical Tg values of PVP, amylose and their blend

PVP/AM composite blend	Experimental Tg values (°C)	Theoretical Tg values (°C)	
		Fox equation	Wood's Equation
Pure PVP	35.83	-	-
PVP/AM (80:20)	43.42	37.08	37.29
Pure Amylose	48.13	-	-

To analyze the effect of Fe<sup>3+</sup>-MMT nanocomposite presence on the thermal stability of PVP/AM blend composite, Thermogravimetric (TG) measurement was performed under the temperature range of 50-600°C with scan rate of 10°C/min under nitrogen atmosphere. The effect of the addition of Fe<sup>3+</sup>-MMT on the thermal stability of PVP/AM films can be observed in the TGA graphs in Fig. 8. The thermal degradation kinetics of the pure components (PVP and amylose) and PVP/AM films with and without the Fe<sup>3+</sup>-MMT nanocomposite loading was analyzed from the non-isothermal Tg profiles, using the Horowitz and Metzger method [44]. The activation energy (E<sub>a</sub>) required for degradation process was calculated from the Eq. 4:

$$\ln \left[ \ln \left( \frac{W_0}{W} \right) \right] = E_a \Theta / RT_{\max}^2 \quad (4)$$

where W is the weight at the temperature chosen, W<sub>0</sub> is the weight at the initial temperature. T<sub>max</sub> is the temperature at maximum rate weight loss. R is the universal gas constant 8.314 J/mol.K and Θ is given by T-T<sub>max</sub>.

The percentage of residual mass at 600°C decreased with the increase of Fe<sup>3+</sup>-MMT loading in the polymer composite matrix. According to the data that presented in Table 5, The PVP/AM/ Fe<sup>3+</sup>-MMT nanocomposite containing of 5wt% of Fe<sup>3+</sup>-MMT, supplied the greatest value for (T90). In general, the addition of Fe<sup>3+</sup>-MMT increased the thermal stability of the PVP/AM film and this behavior sustained by increasing the amount of Fe<sup>3+</sup>-MMT

nanocomposite in the matrix of composite films. Additionally, the obtained T<sub>max</sub> from DTG curves followed this tendency. As seen from the Fig. 9, the highest value of T<sub>max</sub> between the films was observed for PVP/AM which is containing 5wt% of Fe<sup>3+</sup>-MMT nanocomposite (Table 5). Recently, Teodoro et al. reported the thermal degradation process for Cassava starch that was reinforced by acetylated starch nanoparticles (NPAac) [45]. They found that the addition of NPAac in all levels did not affect the value of T<sub>max</sub> and T<sub>onset</sub> in starch films. This result suggesting that the interaction and dispersion of the nanoparticles did not influence the interaction of the water in the starch matrix and therefore could not affect the thermal stability of the films. The activation energies of degradation for all films were determined from the slope of the kinetic plots (Eq. 4) and are reported in Table 5.

#### 4. CONCLUSIONS

In this study, the effect of Fe<sup>3+</sup>-MMT nanocomposite on the mechanical and thermal properties of PVP/AM films has been studied. XRD diffractograms indicated that PVP/AM composite films were intercalated to the interlayer of the MMT nanosheets. These results approved the cation exchange process that occurred and NH<sub>4</sub><sup>+</sup> ions replaced with Fe<sup>3+</sup> cations. Mechanical tests represented significant improvements that were attributed to the uniform dispersion of Fe<sup>3+</sup>-MMT nanocomposite into the polymer network and the covalent interaction between the PVP/AM composite network and Fe<sup>3+</sup> cations. With an increase of Fe<sup>3+</sup>-MMT

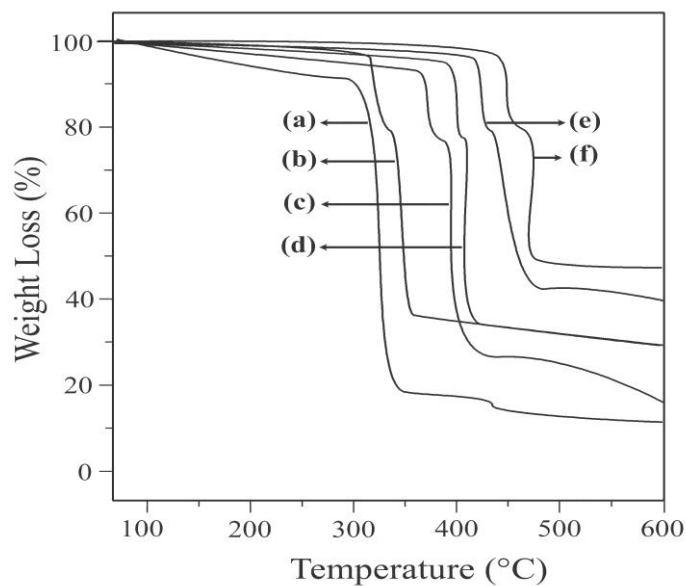


**Fig. 8.** TGA thermograms for (a) pure amylose, (b) pure PVP, (c) PVP/AM blend, and for PVP/AM/  $\text{Fe}^{3+}$ -MMT nanocomposites containing (d) 1wt%, (e) 3wt% and (f) 5wt% of  $\text{Fe}^{3+}$ -MMT.

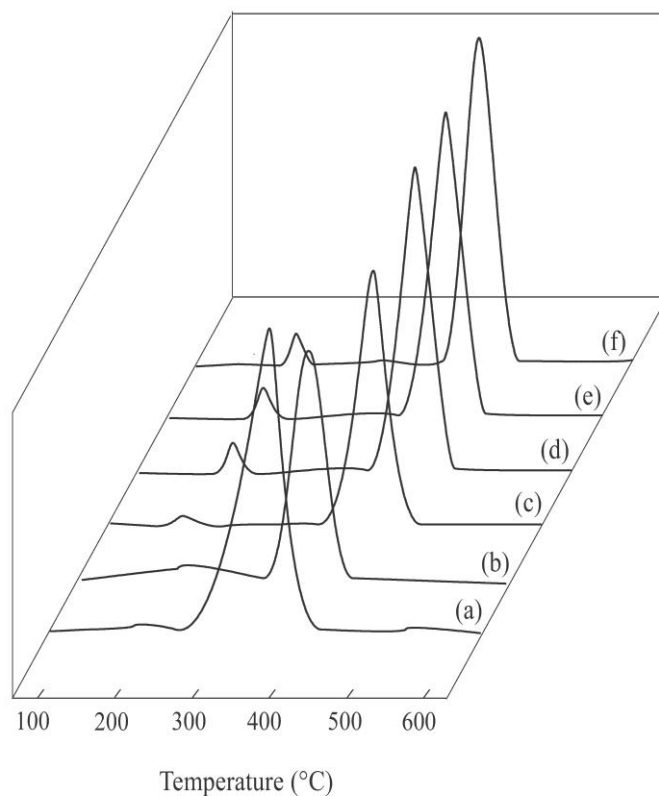


**Fig. 9.** DTG curves as a function of derivative mass%/min for (a) pure amylose, (b) pure PVP, (c) PVP/AM blend, and for PVP/AM/  $\text{Fe}^{3+}$ -MMT nanocomposites containing (d) 1wt%, (e) 3wt% and (f) 5wt% of  $\text{Fe}^{3+}$ -MMT.

**Table 5.** Thermal parameters determined from Thermogravimetric curves for studied samples

Samples	T <sub>90</sub> (°C)	RM600 (%)	T <sub>max</sub> (°C)	T <sub>onset</sub> (°C)	Ea (KJ/mol)
Pure amylose	283	11.04	304	290	123.5
Pure PVP	284	29.40	325	281	44.9
PVP/Amylose	334	15.38	359	331	30.9
PVP/AM/ Fe <sup>3+</sup> -MMT (1wt %)	369	39.94	389	375	187.9
PVP/AM/ Fe <sup>3+</sup> -MMT (3wt %)	391	41.78	404	388	190.8
PVP/AM/ Fe <sup>3+</sup> -MMT (5wt %)	419	47.38	462	446	269.4

content, the tensile strength of the PVP/AM/ Fe<sup>3+</sup>-MMT nanocomposite films increased from 6.4 to 13.0 MPa. The results of thermal investigations show that Fe<sup>3+</sup>-MMT nanocomposite improved the thermal properties of PVP/AM composite films. DSC results showed the shift in onset temperature (T<sub>0</sub>) of PVP/AM/ Fe<sup>3+</sup>-MMT nanocomposite films by adding more Fe<sup>3+</sup>-MMT to the PVP/AM matrix. Also, Thermogravimetry results confirmed the modified thermal properties for PVP/AM/ Fe<sup>3+</sup>-MMT nanocomposite films by calculating the activation energy of different studied samples. The addition of Fe<sup>3+</sup>-MMT increased the thermal stability of the PVP/AM films, and this behavior sustained by increasing the amount of Fe<sup>3+</sup>-MMT nanocomposite in the matrix of composite films.

## 5. ACKNOWLEDGMENT

This paper is retrieved from a research project under the title: Sonocatalytic, photocatalytic, sonophotocatalytic degradation of poly (vinyl pyrrolidone) (PVP) in the presence of TiO<sub>2</sub> nanoparticles that is performed at Islamic Azad University of Ahar. I want to show my deepest gratitude to research assistant of that university.

## REFERENCES:

- [1]. Roy, D., Cambre, J. N., and Sumerlin, B. S., *Prog. Polym. Sci.* 2010, 35, 278–301.
- [2]. Ferro, L., Scialdone, O., and Galia, A., *J. Supercrit. Fluid* 2012, 66, 241–250.
- [3]. Guo, Y., Feng, X., Chen, L., Zhao, Y., and Bai, J., *J. Appl. Polym. Sci.* 2010, 116, 1005–1009.
- [4]. Sharma, K., Kaith, B. S., Kumar, V., Kalia, S., and Swart, H. C., *Polym. Degrad. Stabil.* 2014, 107, 166-177.
- [5]. Ming Yang, J., Zen Wang, H., and Chen Yang, C., *J. Membrane Sci.* 2008, 322, 74–80.
- [6]. Melo, L., Benavides, R., Martínez, G., Da Silva, L., and Paula, M. M. S., *Polym. Degrad. Stabil.* 2014, 109, 343-352.
- [7]. Siviah, K., Hemalatha Rudramadevi, B., and Buddhudu, S., *Ind. J. Pure Appl. Phys.* 2010, 48, 658-662.
- [8]. Ravi, M., Bhavani, S. Pavani, Y., and Narasimha Rao, V. V. R., *Ind. J. Pure Appl. Phys.* 2013, 51, 362-366.
- [9]. Tecante, A., and Doublier, J. L., *Carbohydr. Polym.* 2002, 49, 177-183.
- [10]. Lisa Ryno, M., Yael, L., Peter, M., and Iovine, M., *Carbohydr. Res.* 2014, 383, 82–88.
- [11]. Wu, T., Xie, T., and Yang, G., *Appl. Clay Sci.* 2009, 45, 105-110.
- [12]. Iggui, K., Le Moigne, N., Kaci, M., Cambe, S., Degorce-Dumas, J., and Bergeret, A., *Polym. Degrad. Stabil.* 2015, 119, 77-86.
- [13]. Zha, W., Dae Han, C., Hyun Han, S., Hyun Lee, D. Kon Kim, J., Guoc, M., and Rinaldid, P. L., *Polymer*, 2009, 50, 2411-2423.
- [14]. Arsalani, N., Fattahi, H., and Nazarpour, M., *EXPRESS Polym. Lett.* 2010, 4, 329–338.

- [15]. H. Bel Hadjltaief, P. Da Costa, P. Beaunier, M. Elena Gálvez, M. Ben Zina, *Appl. Clay Sci.* 91-92 (2014) 46-54.
- [16]. Zhou, S., Zhang, C., Hu, X., Wang, Y., Xu, R., Xia, C., Zhang, H., and Song, Z., *Appl. Clay Sci.* 2014, 95, 275-283.
- [17]. He, Y., Wang, X., Wu, D., Gong, Q., Qiu, H., Liu, Y., Wu, T., Ma, J., and Gao, J., *J. Mater. Chem. Phys.* 2013, 142, 1-11.
- [18]. Shujun, W., Jinglin, Y., and Wenyuan, G., *Am. J. Biochem. Biotechnol.* 2005, 1, 207-211.
- [19]. Zhou, X., Wang, R., Zhang, Y., Yoo, S., and Lim, S., *Carbohydr. Polym.* 2013, 95, 227-232.
- [20]. Taghizadeh, M. T., and Abdollahi, R., *Polym. Degrad. Stabil.* 2015, 116, 53-61.
- [21]. Ryno, L. M., Levine, Y., and Iovine, P. M., *Carbohydr. Res.* 2014, 383, 82-88.
- [22]. [22] Kadan, R. S., and Pepperman, A. B., *Cereal Chem.* 2002, 79, 476-480.
- [23]. Wu, Y., Chen, Z. X., Li, X. X., and Wang, Z. J., *LWT – Food Sci. Tech.* 2010, 43, 492-497.
- [24]. Li, D., and Sur, G. S., *J. Ind. Eng. Chem.* 2014, 20, 3122-3127.
- [25]. Zhang, J., Kasuya, K., Takemura, A., Isogai, A., Iwata, T., *Polym. Degrad. Stabil.* 2013, 98, 1458-1464.
- [26]. Zhang, Z., Chen, P., Du, X., Xue, Z., Chen, S., and Yang, B., *Carbohydr. Polym.* 2014, 102, 453-459.
- [27]. Taghizadeh, M. T., and Sabouri, N., *J. Taiwan Inst. Chem. Eng.* 2013, 44, 995-1001.
- [28]. Taghizadeh, M. T., Abbasi, Z., and Nasrollahzade, Z., *J. Taiwan Inst. Chem. Eng.* 2012, 43, 120-124.
- [29]. Almasi, H., Ghanbarzadeha, B., and Entezami, A.A., *Int. J. Biol. Macromol.* 2010, 46, 1-5.
- [30]. Huang, Y., Lu, J., Xiao, C., *Polym. Degrad. Stabil.* 2007, 92, 1072-1081.
- [31]. Muscat, D., Adhikari, B., Adhikari, R., and Chaudhary, D. D., *J. Food Eng.* 2012, 109, 189-201.
- [32]. Nerantzaki, M., Papageorgiou, G. Z., and Bikiaris, D. N., *Polym. Degrad. Stabil.* 2014, 108, 257-268.
- [33]. Matveev, Y. I., van Soest, J. J. G., Nieman, C., Wasserman, L. A., Protserov, V. A., and Ezernitskajal. M., *Carbohydr. Polym.* 2001, 44, 51-60.
- [34]. Zhang, B., Huang, Q., Luo, F., Fu, X., Jiang, H., and Jane, J., *Carbohydr. Polym.* 2011, 84, 1276-1281.
- [35]. Lina, J., Wang, S., and Chang, Y., *Food Hydrocolloid* 2008, 22, 156 – 163.
- [36]. Li, M., Liu, P., Zou, W., Yu, L., Xie, F., Pu, H., Liu, H. and Chen, L., *J. Food Eng.* 2011, 106, 95-101
- [37]. Liu, P., Yu, L., Liu, H., Chen, L., and Li, L., *Carbohydr. Polym.* 2009, 77, 250-253.
- [38]. Liu, P., Yu, L., Wang, X., Li, D., Chen, L., and Li, X., *J. Cereal Sci.* 2010, 51, 388-391.
- [39]. Zhang, Z., Chen, P., Du, X., Xue, Z., Chen, S., and Yang, B., *Carbohydr. Polym.* 2014, 102, 453-459.
- [40]. Guru, G. S., Prasad, P., Shivakumar, H. R., and Rai, S. K., *Int. J. Plast. Technol.* 2010, 14, 234-245.
- [41]. Panayiotou, C. G., *Polym. J.* 1986, 18, 895-902.
- [42]. Baruah, S. D., and Laskar, N. C., *J. Appl. Polym. Sci.* 1996, 60, 649-656.
- [43]. Rao, V., Ashokan, P. V., and Shridhar, M. H., *J. Appl. Polym. Sci.* 2000, 76, 859-867.
- [44]. Horowitz, H. H., and Metzger, G., *Anal. Chem.* 1963, 35, 1464-1468.
- [45]. Paula Teodoro, A., Mali, S., Romero, N., Maria de Carvalho, G., *Carbohydr. Polym.* 2015, 126, 9-16.